Long-ranged spin-glass phase boundary in quasicrystal approximants

Fernand Denoel,[1,*] Karthika K. Thilakan,[2,†] Yu-Chin Huang,[2,‡] Takayuki Shiino,[1,§] Girma Hailu Gebresenbut,[2] Huibo Cao,[3] Ulrich Häussermann,[4] Cesar Pay Gómez,[2] Martin Sahlberg,[2] and Roland Mathieu[1,‖]

[1]*Department of Materials Science and Engineering, Uppsala University, Box 35, 751 03 Uppsala, Sweden*

[2]*Department of Chemistry-Ångström laboratory, Uppsala University, 751 21 Uppsala, Sweden*

[3]*Neutron Scattering Division, Oak Ridge National Laboratory, Oak Ridge, Tennessee 37831, USA*

[4]*Department of Materials and Environmental Chemistry, Stockholm University, 106 91 Stockholm, Sweden*

(Received 15 September 2025; revised 18 May 2026; accepted 13 July 2026; published 4 August 2026)

We report the magnetic structure of the pseudo-Tsai Tb-Au-Si 1/1 approximant crystal (AC), a periodic crystal where the Tb^{3+} magnetic ions are arranged in a bcc packing as icosahedron nodes plus center decoration. While looking seemingly long ranged in dc magnetometry and neutron diffraction experiments, this crystal shows dynamical magnetic behavior consistent with a spin glass, including aging and memory effects. The relevance of the spin chirality subtended by three noncoplanar magnetic moments, and its order and disorder is discussed. The results are compared to those obtained for the regular Tsai Tb-Au-Si 1/1 AC and binary quasicrystals in order to establish an electronic phase diagram illustrating the boundary between long-ranged and short-ranged order in those systems.

DOI: 10.1103/n3yq-b937

I. INTRODUCTION

Quasicrystals (QCs), discovered more than 40 years ago, are crystalline materials aperiodic along at least one dimension [1,2]. Icosahedral quasicrystals (*i*-QCs) are the only type aperiodic along all three dimensions, with the most studied type being the intermetallic Tsai-type QCs, which can contain magnetic lanthanide elements, exhibiting $4f$ shell magnetism. Approximant crystals (ACs) are crystals which possess the same local arrangement of atoms as their QC counterpart, albeit arranged in a periodic manner [3,4]. This enables a unique structure where magnetic ions arranged in nearly perfect icosahedra can exist in a periodic crystal, surrounded only by nonmagnetic ions and thus giving rise to unique magnetic structure and a diverse set of magnetic behaviors governed by the Ruderman-Kittel-Kasuya-Yosida (RKKY) interaction [5,6]. The 1/1 type of ACs have icosahedra atomic decorations of lanthanide elements arranged in a body-centered-cubic (bcc) lattice, as illustrated in Fig. 1(a). If a stable QC phase exists, one or more stable AC counterparts with similar composition can also be synthesized, but the reverse is not always true.

The ternary Tb-Au-Si system is one such system, where the 1/1 AC phase is achievable but without a stable QC counterpart. However, in this ternary system, a structural change unique to the 1/1 ACs and absent from QCs can be induced depending on the synthesis conditions, the pseudo-Tsai type of structure [4,7], which allows to add one extra magnetic lanthanide ion at the center of the bcc icosahedral lattice, with the starting materials used for the synthesis allowing any occupancy between 0% to 100% cluster centers (CCs). We refer to these systems as TAS(0) and TAS(100), respectively. TAS(0) is a regular Tsai phase (0% CC occupation) while TAS(100) with full pseudo-Tsai occupation, has a Tb rare earth (RE) metal at the CC of every icosahedra (12 Tb^{3+} ions).

In the present article, we first recall specific features of the magnetic behavior of the pure Tsai and pure pseudo-Tsai phases. In short, TAS(0) and TAS(100) display magnetization curves as a function of temperature and magnetic field which are typical of noncoplanar ferrimagnets [8], with a sharp onset of magnetization when the magnetic order sets in [see also Fig. 1(b)]. However, TAS(0) is a frustrated noncoplanar ferrimagnet [8] displaying glassiness, while TAS(100) behaves dynamically as a canonical spin glass [9,10]. In order to explain the different ground states of the two systems [9], we have here determined the magnetic structure of TAS(100) using single-crystal neutron diffraction (SCND). The magnetic structure and magnitude of the magnetic moments are compared to those obtained earlier for TAS(0) and other ACs [11]. We discuss how the CC moments affect chirality and magnetic order, and sketch an electronic phase diagram of the Tb-Au-Si system as a function of CC occupancy. The results are compared to those of binary *i*-Tb-Cd quasicrystals,

*Contact author: fernand.denoel@gmail.com

†Contact author: karthika.kariattukarakaran-thilakan@kemi.uu.se

‡Present address: Department of Materials and Manufacturing, Jönköping University, Box 1026, 551 11 Jönköping, Sweden.

§Present address: Institut de Ciència de Materials de Barcelona (ICMAB-CSIC), Carrer dels Til·lers, 08193 Cerdanyola del Vallès, Spain.

‖Contact author: roland.mathieu@angstrom.uu.se

Published by the American Physical Society under the terms of the Creative Commons Attribution 4.0 International license. Further distribution of this work must maintain attribution to the author(s) and the published article's title, journal citation, and DOI. Funded by Bibsam.

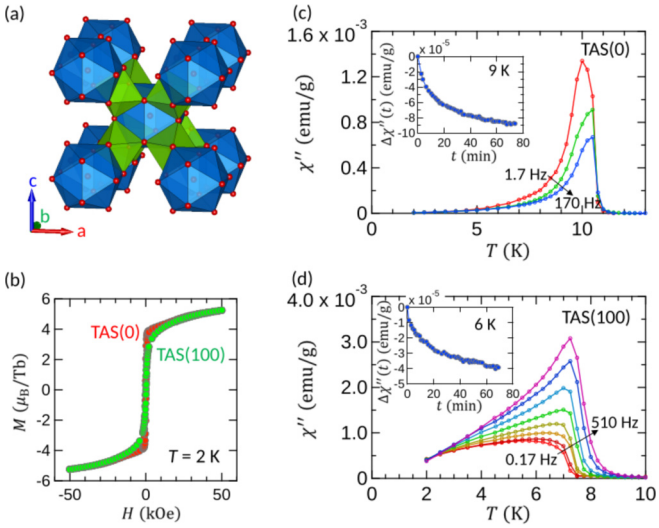


FIG. 1. (a) Body-centered arrangement of icosahedra with Tb atoms occupying the vertices and the cluster center in the 1/1 AC. The icosahedra are shown as blue polyhedra, and the corner-sharing interstitial octahedral units are highlighted in green; for details, see the main text and Ref. [4]. (b) Magnetization M vs magnetic field H curves at $T = 2$ K for TAS(0) and TAS(100). Out-of-phase component of the ac susceptibility χ'' vs temperature for (c) TAS(0) and (d) TAS(100); the respective insets show the time dependence of χ'' [plotted as $\chi''(t) - \chi''(t = 0)$] at a constant temperature after a quench (rapid cooling) from a reference temperature in the paramagnetic phase; ac excitation $h = 4$ Oe and frequency $f = 1.7$Hz.

which were interestingly found to display similar magnetic behavior.

II. EXPERIMENTAL METHODS

Single-crystal specimens (masses$\sim$ 10mg) of TAS(0) and TAS(100) were prepared from solution growth according to Ref. [4], using reaction mixtures with compositions $Tb_5(Au_{0.79}Si_{0.21})_{95}$ and $Tb_{15}(Au_{0.79}Si_{0.21})_{85}$, respectively.

Single-crystal neutron diffraction (SCND) measurements on TAS(100) were carried out at the HB-3A four-circle diffractometer at the High Flux Isotope Reactor (HFIR), Oak Ridge National Laboratory, USA [12]. A single crystal of approximate dimensions 3 × 4mm was chosen for the experiment (mass$\sim$ 275mg). The neutron data were collected at two temperatures: 10 K, corresponding to the paramagnetic state, and 5 K, just below the magnetic transition temperature. A neutron wavelength of 1.54 Å was used for all measurements. Nuclear and magnetic structure refinements were performed using JANA2020 software package [13]. Both samples used in magnetometry and neutron diffraction experiments were independently identified as the TAS(100) phase based on their lattice constants and CC occupancies, as determined from x-ray diffraction (XRD) and neutron refinements. For example, the refined lattice constant from the neutron data at 5 K is 14.540(3) Å (see Supplemental Material [14]), which is consistent with TAS(100) [4]. The crystals also display similar magnetic properties, as seen in the Supplemental Material (Fig. S4) [14].

The dc magnetization and ac magnetic susceptibility data were collected using a magnetic properties measurement system (MPMS XL) superconducting quantum interference device (SQUID) magnetometer from Quantum Design.

III. RESULTS AND DISCUSSIONS

A. Magnetic behavior of Tsai and pseudo-Tsai phases

Looking at the behavior of the out-of-phase component of the ac susceptibility χ'' depicted in Figs. 1(c) and 1(d) (main frames), one can see that the temperature onset of χ'' is frequency independent for TAS(0), as expected for a long-ranged ordered system. Some frequency dependence is observed below the maximum of χ''. In contrast, a significant frequency-dependent temperature onset of χ'' is observed for TAS(100)—see Fig. 1(d). This behavior is reminiscent of spin glasses (SGs) [15], whose spin configuration may be disturbed by perturbations such as temperature changes, yielding dynamical effects [16]. While the frequency dependence of the onset of χ'' reflects the onset of nonequilibrium dynamics and critical slowing down at the SG phase transition (if it exists), magnetic frustration and glassiness may be evidenced by the dc or ac relaxation (equilibration, or "aging" [15]) of the system. Interestingly, as illustrated in the insets of Figs. 1(c) and 1(d), not only TAS(100), but also TAS(0) displays the characteristic SG-like relaxation (see Ref. [9]).

This suggests that TAS(0) is not a regular ferrimagnet (FiM). Some of us have shown earlier that TAS(0) is likely to be a magnetically frustrated FiM [9]. Such phases typically evolve into SG ones at lower temperatures and the system is deemed a reentrant SG [17]. Interestingly, the FiM phase of a magnetic frustrated FiM may show glassy properties such as aging, but its spin configuration is not as robust against, e.g., temperature changes as those of SGs, which may "remember" the aging which may have occurred at another temperature (memory, see Refs. [17,18]). TAS(100), on the other hand, displays archetypical properties of SGs (aging, memory, and rejuvenation [10]) and is likely to undergo a spin-glass phase transition [9].

B. Neutron diffraction and magnetic structure for TAS(100)

The nuclear structure was refined using data collected at 10 K and confirmed that the compound crystallizes in the body-centered-cubic (bcc) space group $Im\bar{3}$, consistent with the 1/1 Tsai-type approximant structure (see Supplemental Material [14] for details). The unit cell is composed of concentric polyhedral shells surrounding a central atom, arranged in the sequence Tb atom (as the cluster center), pentagonal dodecahedron, icosahedron, icosidodecahedron, and rhombic triacontahedron [4].

The temperature dependence of the $(0, 0, 2)$ Bragg reflection was monitored to track the onset of magnetic ordering. A clear increase in intensity was observed below 8 K, indicating the emergence of magnetic scattering and confirming the magnetic nature of the compound (see Fig. S1 [14]). A rocking curve (ω scan) was performed for the $(0, 0, 2)$ reflection at both 10 and 5 K (Fig. S2 [14]). The appearance of a well-defined Bragg peak at 5 K, absent at 10 K, confirms that this reflection arises predominantly from magnetic ordering.

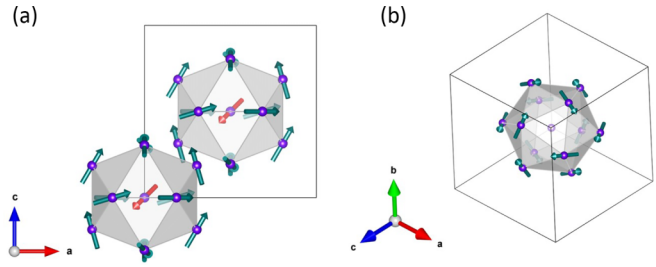


FIG. 2. Refined magnetic structure of TAS(100) at 5 K (a) shows the Tb magnetic moments and their arrangements on the atomic clusters. Only two clusters in the cubic unit cell are shown here for clarity. Green colored arrows represent moments at the ICS, and red colored arrows for the CC Tb moment. Moments at the ICS and CC are scaled to have the same magnitude for clarity. (b) A single atomic cluster viewed from the [111] direction.

Magnetic structure determination was conducted using neutron data collected at 5 K. A Magnetic space group (MSG) analysis was performed using the representation analysis tool in JANA2020. All the MSGs related to the parent nuclear structure were tested and the lowest R value was obtained for the rhombohedral $R\bar{3}$ space group. An increase in the intensity of selected nuclear Bragg peaks indicated the onset of long-range magnetic order, and the magnetic propagation vector, $\mathbf{k} = (000)$. These magnetic reflections obey the same selection rule as the nuclear structure (i.e., $h + k + l = 2n$), suggesting that the magnetic structure retains the bcc symmetry of the underlying lattice. In the $R\bar{3}$ space group, the Tb atoms at the icosahedral shell (ICS) sites split into two crystallographically inequivalent positions, giving Tb1_1 and Tb1_2. Refinement of the magnetic structure was carried out on the square of the observed structure factor amplitudes ($|F_{\text{obs}}|^2$). Atomic coordinates, atomic displacement parameters (ADPs), and the site occupancies were fixed during magnetic structure refinement. The magnetic moments at the icosahedral Tb1_1 and Tb1_2 sites were constrained to have equal magnitudes, while the moment on the central Tb atom was allowed to vary. Results from the magnetic structure determination and refinement are given in detail in the Supplemental Material, including Fig. S3 [14].

In agreement with previous studies on 1/1 Tsai-type approximants [8,19–21], the magnetic structure exhibits a noncoplanar, noncollinear arrangement of moments with a characteristic whirling pattern around the [111] crystallographic direction at the ICS (see Fig. 2). The refined magnetic moment for the Tb atoms in the icosahedron is $6.04(7)\mu_B$, while the central Tb atom exhibits a reduced moment of $2.2(6)\mu_B$. The theoretically expected moment for Tb^{3+} is 9 μ_B ($g_J J\mu_B = 9\mu_B/Tb^{3+}$). The reduction in moment magnitude at the ICS sites can be attributed to crystal electric field (CEF) effects, as well as to the fact that the measurements were conducted just below the magnetic transition temperature, where static magnetic order may not be fully developed. The strong suppression of the moment at the CC may be due to partial magnetic disorder or frustration at that site. In addition to the magnetic Bragg peaks, weak diffuse scattering features were also observed in the SCND data. The tail between 8 and 10 K in the temperature-dependent intensity plot (Fig. S1 [14]) suggests potential critical diffuse scattering of a magnetic nature.

TABLE I. comparison of Tb magnetic moments at the icosahedral shell and cluster center for TAS(0) and TAS(100).

Compound	Moment Size (μ_B)	
	ICS	CC
TAS(0)	8.28 (1)	
TAS(100)	6.04 (7)	2.2 (6)

Previous neutron diffraction studies on Tb-Au-Si compounds [8,11] have reported whirling magnetic orders around the icosahedral threefold axis, with a noncollinear noncoplanar spin arrangement. For example, in a compound with 14% central Tb occupancy [TAS(14)], the refined moments were $4\mu_B$ at the icosahedral sites and $8.66\mu_B$ at the cluster center (CC). This was attributed to the significant magnetic interaction between the CC Tb atom with the icosahedral Tb atoms. It is important to note, however, that the determination of moment magnitudes in this case was based on powder neutron diffraction, which, while highly effective for revealing average magnetic structures, may limit the resolution of site-specific magnetic moment details, particularly in complex noncollinear magnetic structures. In contrast, the Ho-Au-Si compound with 52% CC occupancy, referred to as HAS(52), exhibits a strongly quenched magnetic moment at the CC, refined to $0.85(42)\mu_B$. This quenching has been attributed to the highly symmetric nature of the central $2a$ Wyckoff position, where the net magnetic field from surrounding atoms may effectively cancel out, resulting in disordered central moments due to thermal fluctuations [11].

In the present case of TAS(100), all cluster centers are fully occupied by Tb atoms. The central Tb atoms are in close proximity to the surrounding icosahedral Tb atoms, with interatomic distances shorter than those between neighboring icosahedral sites [22]. This spatial arrangement suggests significant magnetic exchange interactions between the central and icosahedral Tb atoms. TAS(100) exhibits behavior reminiscent of HAS(52), where the magnetic moments at the cluster centers appear frustrated or only partially ordered. In the case of TAS(0), the magnetic moments at the ICS were found to have an average magnitude of $8.28\mu_B$. Table I shows the comparison of long-range ordered moment sizes for TAS(0) and TAS(100). The spins tend to appear perpendicular to the pseudofivefold axis of the icosahedral shell [11] for TAS(0). A similar spin alignment tendency is observed in TAS(100), indicating a consistent easy-axis anisotropy of Tb atoms at the icosahedral shell.

It is interesting to note that the present neutron data on TAS(100) evidence both long-ranged (sharp magnetic Bragg peaks) and short-ranged (diffuse scattering) magnetic correlation, as may be observed in systems with several magnetic sublattices such as ferrimagnets, and reentrant glassy systems [23–25]. The coexistence here may reflect the close proximity of the glassy phase of TAS(100) to ferrimagnetic order, yielding a ferrimagnetic correlation along the glassy one, as observed in the glassy phase of reentrant systems [26] (see below for more discussion about the ferrimagnetic-spin-glass boundary).

C. Chirality

There are only icosahedral Tb atoms in the case of TAS(0). The scalar and vector chiralities associated with noncoplanar spins were calculated from the magnetic structure determined by SCND [9,11]. TAS(0) was found to display chiral order, with the sign of the scalar spin chirality $\chi_{ijk} = \mathbf{S}_i \cdot (\mathbf{S}_j \times \mathbf{S}_k)$ alternating from positive to negative between two neighboring edge-sharing triangular faces of the octahedral units (in green color in Fig. 1; see also Ref. [9]). The vector spin chirality was also found to point along the [111] direction in an uniaxial fashion (see Ref. [9] and its Supplemental Material).

It is instructive to consider the geometrical arrangement of spins within icosahedral clusters. As illustrated in Fig. 3(a), the presence of a CC-Tb moment introduces additional internal triangular units of spin chirality inside the icosahedron. Because the icosahedron has 30 edges, there are also 30 such inner triangles that involve the CC-Tb moment. One representative triangle, formed by the three spins labeled $(0, i, j)$, is highlighted in Fig. 3(a). These internal isosceles triangles are nearly equilateral, since the ratio between the circumscribed-sphere radius and the edge length of the icosahedron is approximately 0.95:1. Therefore, the TAS(100) system contains triangular units that can potentially induce magnetic frustration not only on the surface of the icosahedron but also inside it.

Given the unique geometrical structure of this system, a natural question here is what kind of degrees of freedom can be frozen. One possible intriguing scenario is the freezing of scalar spin chirality, in analogy to Kawamura's chirality scenario originally proposed for Heisenberg spin systems with weak anisotropy [27]. In the present case, however, the icosahedral Tb ions are subject to CEF effects that are expected to restrict their local spin degrees of freedom to Ising-like with respect to their ordered directions [28,29]. Note that the magnetic entropy of TAS(0) and TAS(100) reaching nearly $R \log 2$ above the ordering temperatures indicates a CEF ground-state doublet [11]. The SG behavior of TAS is also qualitatively similar to that of Ising SG [9]. The actual ordered Tb moments through RKKY interactions form noncoplanar configurations primarily due to the geometrical arrangement of the cluster combined with the local anisotropy, within which scalar spin chiralities are naturally defined. The situation for the CC-Tb site remains unclear, although it may also possess Ising-like degrees of freedom along the [111] axis.

The CC-Tb ions are surrounded by the dodecahedral shell, which contains chemically disordered Au/Si mixed sites. Such inherent disorder may affect the local exchange couplings between the CC-Tb and icosahedral Tb moments, leading to spatially nonuniform local magnetic environments for the CC-Tb moments. For simplicity, we illustrate two representative Ising-like configurations with opposite orientations of the CC-Tb moment—along [111] and $[\bar{1}\bar{1}\bar{1}]$—while keeping the icosahedral Tb moments fixed, as depicted in Fig. 3(a). We note that these two configurations are intended as examples of the possible local magnetic states of the CC-Tb moments. In this picture, the signs of the scalar spin chiralities on the inner triangles (red versus blue highlighted triangles) depend on the CC-Tb orientation. Within the framework of the present chirality scenario, the scalar spin chiralities associated with the inner triangular units may become locally frozen at low temperatures because of the combined effects of geometrical frustration and spatially nonuniform exchange couplings. As a consequence, through the coupling between chirality and

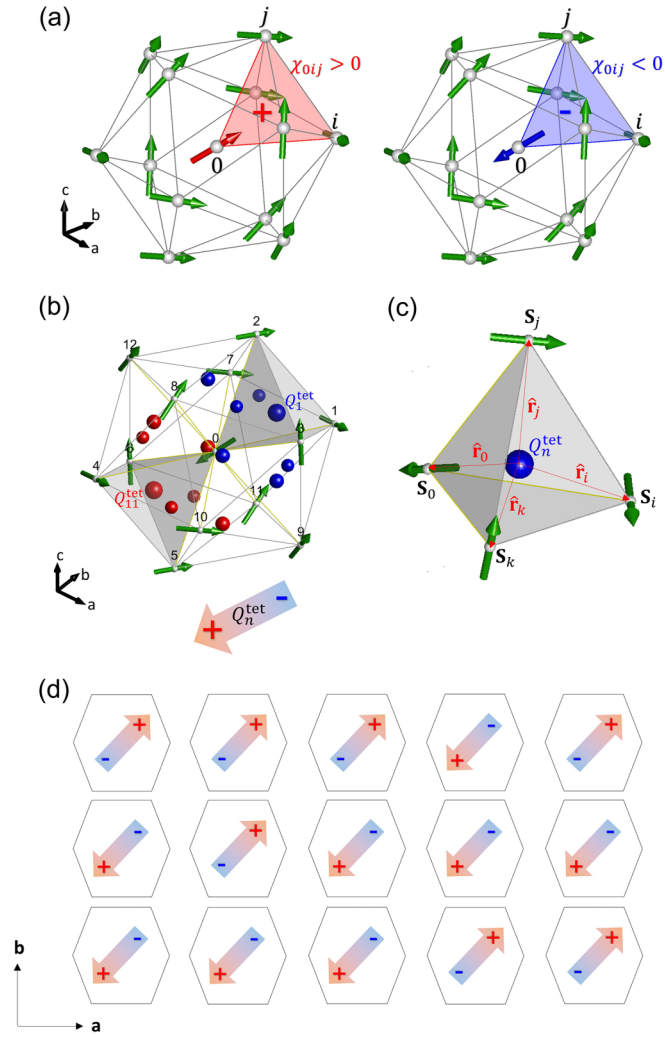


FIG. 3. Spin chirality and tetrahedral magnetic charge in the icosahedral cluster with CC-Tb. (a) Two representative spin configurations of the icosahedral TAS(100) cluster, characterized by opposite orientations of the cluster-center (CC) Tb moment: along the [111] direction (left) or the $[\bar{1}\bar{1}\bar{1}]$ direction (right). The red and blue shaded triangles highlight representative scalar spin chiralities χ_{ijk}, whose signs ($\chi_{ijk} > 0$ and $\chi_{ijk} < 0$) depend on the CC-Tb moment orientation. (b) Visualization of the tetrahedral magnetic charges Q_n^{tet} inside the icosahedral cluster. The sphere color encodes the sign of the charge—red for $Q_n^{tet} > 0$ and blue for $Q_n^{tet} < 0$—while the sphere size represents the relative magnitude of $|Q_n^{tet}|$. For clarity, only the two tetrahedra ($n = 1$ and $n = 11$) are highlighted in gray. Some spheres are barely visible because the corresponding $|Q_n^{tet}|$ is much smaller than the others. (c) Definition of the tetrahedral magnetic charge. The red arrows depict the unit vectors $\hat{\mathbf{r}}_l$ pointing from the tetrahedron center toward the four Tb sites $l = 0, i, j, k$. (d) Schematic illustration of the real-space random pattern of tetrahedral magnetic-charge polarization in the icosahedral units. In the present TAS(100) system, the polarization direction tends to align approximately along the [111] axis.

TABLE II. Indices of the three icosahedral Tb sites (i, j, k) forming the nth tetrahedron together with the CC-Tb site (0). The index numbers are indicated in Fig. 3(b).

n	(i, j, k)	n	(i, j, k)
1	(1,2,3)	11	(4,6,5)
2	(1,3,9)	12	(4,5,10)
3	(1,9,11)	13	(4,10,8)
4	(1,11,7)	14	(4,8,12)
5	(1,7,2)	15	(4,12,6)
6	(2,7,12)	16	(5,6,11)
7	(2,12,8)	17	(5,11,9)
8	(2,8,3)	18	(5,9,10)
9	(3,8,10)	19	(6,7,11)
10	(3,10,9)	20	(6,12,7)

spin mediated by magnetic anisotropy, the spin degrees of freedom may also become frozen, leading to a random distribution of local CC-Tb configurations. This provides a possible microscopic route toward the glassy behavior observed in TAS(100). It should be noted that the CEF ground state of the CC-Tb is expected to be different from that of the icosahedral Tb moment. For simplicity, Fig. 3(a) depicts equal moment magnitudes for the CC and icosahedral Tb sites.

In addition to the chirality discussed above, the peculiar geometry of the icosahedral Tb network with the CC-Tb also allows one to define another local quantity that is a tetrahedral magnetic charge. For each of the 20 tetrahedra formed by the central Tb moment and three surrounding icosahedral Tb sites, we define the quantity

$$Q_n^{\text{tet}} = -\sum_{l=0,i,j,k} \mathbf{S}_l \cdot \hat{\mathbf{r}}_l, \tag{1}$$

where $\hat{\mathbf{r}}_l$ is the unit vector pointing from the tetrahedron center toward site l. This quantity is the lattice analog of the divergence of local magnetization and represents an emergent magnetic charge located within each tetrahedral unit. This introduction of the tetrahedral magnetic charge is motivated by the pyrochlore spin-ice systems [30], where the network of corner-sharing tetrahedra hosts magnetic frustration and the emergent magnetic-monopole excitations violating the two-in-two-out ice-rule state have been an intriguing subject of study. In the present TAS(100) system, the face-sharing tetrahedra are considered. Figures 3(b) and 3(c) illustrate that the icosahedral cluster in TAS(100) naturally hosts such internal magnetic charges, whose signs reflect how the local spin configuration converges toward or diverges from the tetrahedral center. The combination of the indices (i, j, k) for nth tetrahedral magnetic charge Q_n^{tet} is presented in Table II. Within a single icosahedral cluster, the sum of the 20 tetrahedral magnetic charges is zero, $\sum_{n=1}^{20} Q_n^{\text{tet}} = 0$.

A remarkable feature of this system is that changing the CC-Tb moment from [111] to $[\bar{1}\bar{1}\bar{1}]$ (and vice versa) reverses the signs of Q_n^{tet}, leading to opposite patterns of magnetic charge polarization inside the same geometrical cluster. This effect is visualized schematically in Fig. 3(d). The emergent magnetic charges Q_n^{tet} do not need to order uniformly, while the icosahedral Tb moments are long-range ordered. Instead, because these charges are constrained by the icosahedral geometry and by the competition among multiple exchange paths, they can form a frustrated network of monopolelike excitations. If the orientations or local configurations of the CC-Tb moments vary spatially over the sample—as may be promoted by the Au/Si disorder on the dodecahedral shell—the pattern of Q_n^{tet} becomes spatially nonuniform, as illustrated in Fig. 3(d). Such disorder in magnetic-charge polarization, superimposed on the long-range magnetically ordered background, could also provide a route toward slow relaxation and aging phenomena.

This picture suggests that TAS(100) may realize a state in which long-range magnetic correlations coexist with an internal network of frustrated tetrahedral magnetic charges tied to the cluster geometry. Because these charges are defined by the local divergence of the spin configuration, their fluctuations are closely related to the chirality degrees of freedom. The freezing of the scalar chiralities on the inner triangular units [Fig. 3(a)] and the freezing of the tetrahedral magnetic charges [Figs. 3(b)–3(d)] may therefore be regarded as two complementary descriptions of the same underlying frustration inherent to the icosahedral cluster. We speculate that the aging behavior observed in TAS(100) originates from the slow dynamics of this emergent network of magnetic charges and chiral units, both of which experience competing interactions and local disorder in the presence of a long-range magnetically ordered state.

D. Long-ranged versus spin-glass phase boundary

In the electronic phase diagram or archetypical spin glasses such as the "Heisenberg-like" Cu(Mn) alloys or anisotropic "Ising" $Fe_{0.5}Mn_{0.5}TiO_3$ oxide [15], one may find long-ranged ordered phases such as ferromagnetic or antiferromagnetic ones, which are stabilized at higher or lower concentrations of magnetic atoms/ions—determining the magnitude of the magnetic interaction and frustration. Also, as depicted in Fig. 4(a), reentrant spin-glass phases may exist—see, e.g., the electronic phase diagram of the $(Fe_xNi_{1-x})_{75}P_{16}B_6Al_3$ alloys [31] as function of Fe (x) content. The spin-glass phases define a region in the diagram (right-hand side) which shows a paramagnetic (PM) to SG transition as a function of the temperature. The long-ranged ordered (here FiM) phases define another region (left-hand side) with PM to FiM transitions. The two are separated by a third region in which the system behaves as a reentrant spin glass, with a succession of phase transitions: PM to FiM to SG. In the latter case, the low-temperature reentrant spin-glass phase may include a background long-ranged (ferrimagnetic) correlation originating from the higher-temperature magnetically ordered state, surviving at low temperatures in the spin-glass one. That long-ranged correlation is detected in neutron experiments, as suggested by our SCND results, and discussed in Ref. [32]. It is also worth mentioning that the whirling (chiral) spin structure in the icosahedral cluster could play a role analogous to that of the "vortexlike defects" observed in reentrant SGs [32]. Consequently, such a whirling spin structure in the present system may facilitate the emergence of frustrated or glassy behavior while maintaining long-range order.

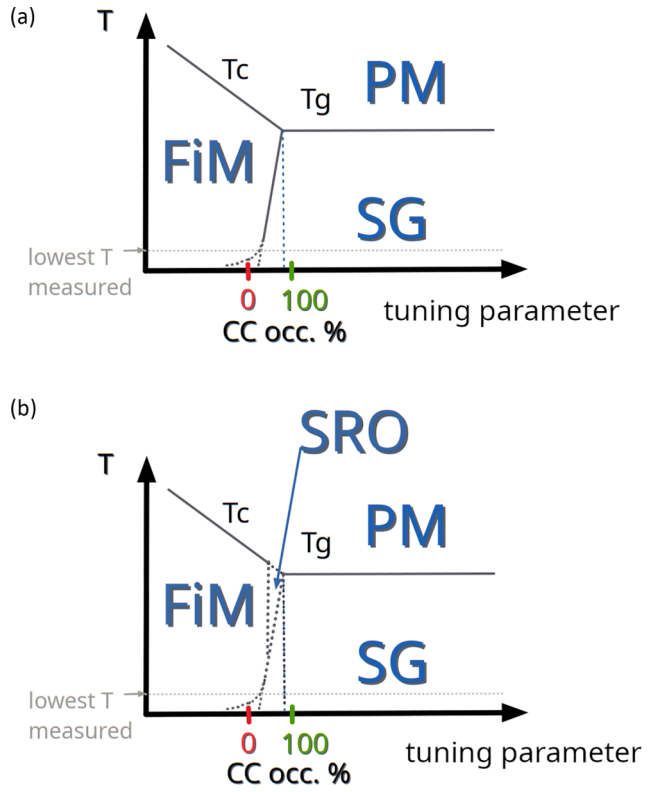


FIG. 4. (a) Electronic phase diagrams mimicking the results on dilute metallic alloys showing FiM (or ferromagnetic) and SG phases (see Ref. [31] for real diagrams; the tuning parameter may be a chemical composition or the resulting magnetic interaction strength); T_c: the FiM transition temperature. T_g the spin-glass transition temperature. The location of TAS(0) and TAS(100) in the diagrams is indicated. (b) Modified version of (a), considering a magnetic phase with short-ranged order (SRO) between FiM and SG phases.

We may speculate here that TAS(0) is close to the FiM-SG phase boundary [see Fig. 4(a)] as it shows long-ranged magnetic order, and at the same time evidence of magnetic frustration and dynamical magnetic features. As suggested in the diagram, TAS(0) could even be a reentrant spin glass if a SG phase transition were to occur below 2 K, the lowest temperature measured in our magnetometry experiments. In the case of TAS(100), the long-ranged order is destabilized, as hinted by the magnetic ordering changing from FiM to SG, and being shifted to lower temperatures ($\approx$ 11K down to 7 K). Also, the susceptibility data above the transition follow a Curie-Weiss behavior, with Θ_{CW} decreasing from 10.2 K for TAS(0) to 5.9 K for TAS(100) [4]. We speculate that TAS(100) is also close to the FiM/SG boundary, as the $M(H)$ data at low T for TAS(100) is relatively similar to that of TAS(0) (see Fig. 1), and SCND evidence well-defined magnetic peaks.

As mentioned in the neutron diffraction section, a system with partial CC occupancy, TAS(14), was synthesized. The static and dynamical magnetic properties of TAS(14) were investigated in Refs. [9,11]. The temperature onset of magnetic ordering for TAS(14) is between that of TAS(0) and TAS(100) ($\approx$ 9K), yet the ac susceptibility and dynamical magnetic properties are closer to those of TAS(100) [9]. TAS(14) is not a long-ranged ferrimagnet. It is likely that TAS(14) is a glassy system with short-ranged magnetic order, albeit without a spin-glass phase transition.

Looking at Fig. 4(a) one would expect all the systems with occupancies between 0 and 100 shall exhibit a reentrant spin-glass behavior (PM to FiM to SG). However, as mentioned above for TAS(14), this is not observed. This suggests that the low-temperatures SG and FiM phases are separated by an intermediate phase with short-range order (SRO), which may evolve into a SG at lower temperatures, as sketched in Fig. 4(b). Such SRO phase separating two magnetically frustrated phases has been observed in temperature-chemical composition electronic phase diagrams of alloys and oxides, mainly between the spin-glass phase of a reentrant spin glass and a spin-glass one [33,34]. The phases at play in the case of the Tb-Au-Si 1/1 ACs would be the frustrated FiM phase of TAS(0) and the SG one of TAS(100).

Interestingly, in binary quasicrystals such as *i*-RE-Cd, the *i*-Gd-Cd QC was found to show a PM to SG phase transition as a function of the temperature [35], while the closely related *i*-Tb-Cd displays the succession: PM to SRO to SG [36], i.e., an evolution with temperature of a SRO to SG, akin to the behavior displayed by TAS(14) [9]. Here, the "tuning parameter" used in Fig. 4 would, e.g., be the size of the RE atoms. Unfortunately the *i*-Dy-Cd QC orders at too low temperatures to be investigated by magnetometry by us and confirm this trend (see Ref. [36] and its Supplemental Material).

The results hence suggest specific short- and long-ranged ordered magnetic states (here, SG and FiM) for ACs/QCs, e.g., long-ranged phases might show dynamical magnetic features owing to the magnetic frustration, while glassy ones may be affected by surviving long-range magnetic correlation. Ho-Au-Si 1/1 AC with no CC occupancy [HAS(0)] orders at lower temperatures than TAS(0); hence as for the *i*-Dy-Cd QC, detailed studies are not possible. However, HAS(0) was found to display similar ac relaxation than TAS(0), i.e., signs of magnetic frustration of the long-ranged FiM phase [9].

IV. CONCLUSION

The magnetic structure of a pseudo Tsai Tb-Au-Si 1/1 AC [TAS(100), 100% CC occupancy] was determined using single-crystal neutron diffraction. The icosahedral Tb moments were found smaller than for the Tsai 1/1 AC [TAS(0), 0% CC occupancy], while the CC ones were determined to be relatively small, $\approx 2.2\mu_B$ at 5 K. The relatively random orientation of the CC moments may perturb the long-ranged ferrimagnetic order established for 0% CC occupancy, yielding a spin-glass behavior for TAS(100).

The magnetic properties of the two Tb-Au-Si 1/1 ACs are determined by the interplay of local structure, chemical disorder, geometrical frustration, and crystalline electric-field (CEF) effects. These may affect the spin dimensionality of the systems. Yet, interestingly, we speculate that the magnetic structure and its order-disorder may be described using the spin chirality subtended by the noncoplanar magnetic moments. The magnetic structure was also used to estimate the tetrahedral magnetic charges within icosaheral clusters and their order/disorder.

By comparing the two Tb-Au-Si 1/1 ACs and related quasicrystals, we describe in detail the long-ranged/short-ranged ferrimagnetic/spin-glass phase boundary in these systems. Further understanding may require studying the diffuse scattering in SCND and/or inelastic neutron spectroscopy.

ACKNOWLEDGMENTS

We thank the Knut and Alice Wallenberg Foundation (Grant No. KAW 2018.0019) and the Swedish Foundation for Strategic Research (SSF) through SwedNess (Grant No. GS1715-0008). This research used resources at the High Flux Isotope Reactor, a DOE Office of Science User Facility operated by the Oak Ridge National Laboratory. The beamtime was allocated to HB-3A DEMAND instrument on proposal No. IPTS-26175.1. We also thank Dr. Matthias Gutmann for the helpful discussions on magnetic structure analysis.

DATA AVAILABILITY

The data that support the findings of this article are not publicly available. The data are available from the authors upon reasonable request.

[1] D. Levine and P. J. Steinhardt, Quasicrystals: A new class of ordered structures, Phys. Rev. Lett. **53**, 2477 (1984).

[2] A. I. Goldman, Magnetism in icosahedral quasicrystals: Current status and open questions, Sci. Technol. Adv. Mater. **15**, 044801 (2014).

[3] T. Fujiwara and Y. Ishii, *Quasicrystals* (Elsevier Science, Amsterdam, 2007), Vol. 3.

[4] G. Gebresenbut, T. Shiino, D. Eklöf, D. C. Joshi, F. Denoel, R. Mathieu, U. Häussermann, and C. Pay Gómez, Atomic-scale tuning of Tsai-type clusters in RE–Au–Si systems (RE = Gd, Tb, Ho), Inorg. Chem. **59**, 9152 (2020).

[5] S. Suzuki, A. Ishikawa, T. Yamada, T. Sugimoto, A. Sakurai, and R. Tamura, Magnetism of Tsai-type quasicrystal approximants, Mater. Trans. **62**, 298 (2021).

[6] F. Labib, K. Nawa, S. Suzuki, H. C. Wu, A. Ishikawa, K. Inagaki, T. Fujii, K. Kinjo, T. J. Sato, and R. Tamura, Unveiling exotic magnetic phase diagram of a non-Heisenberg quasicrystal approximant, Mater. Today Phys. **40**, 101321 (2024).

[7] M. L. Fornasini, P. Manfrinetti, D. Mazzone, and S. K. Dhar, Crystal structure and magnetic properties of the compounds $Yb(Zn, Al)_6$ and $YbZn_6$, Z. Naturforsch. B **63**, 237 (2008).

[8] T. Hiroto, T. J. Sato, H. Cao, T. Hawai, T. Yokoo, S. Itoh, and R. Tamura, Noncoplanar ferrimagnetism and local crystalline-electric-field anisotropy in the quasicrystal approximant $Au_{70}Si_{17}Tb_{13}$, J. Phys.: Condens. Matter **32**, 415802 (2020).

[9] T. Shiino, F. Denoel, G. H. Gebresenbut, C. P. Gómez, P. Nordblad, and R. Mathieu, Nonequilibrium dynamical behavior in noncoplanar magnets with chiral spin texture, Phys. Rev. B **105**, L180409 (2022).

[10] H. Kawamura and T. Taniguchi, Spin glasses, in *Handbook of Magnetic Materials*, edited by K. Buschow (Elsevier, 2015), Vol. 24, pp. 1–137.

[11] G. H. Gebresenbut, T. Shiino, M. S. Andersson, N. Qureshi, O. Fabelo, P. Beran, D. Qvarngård, P. Henelius, A. Rydh, R. Mathieu, *et al.*, Effect of pseudo-Tsai cluster incorporation on the magnetic structures of *R*-Au-Si (*R* = Tb, Ho) quasicrystal approximants, Phys. Rev. B **106**, 184413 (2022).

[12] B. C. Chakoumakos, H. Cao, F. Ye, A. D. Stoica, M. Popovici, M. Sundaram, W. Zhou, J. S. Hicks, G. W. Lynn, and R. A. Riedel, Four-circle single-crystal neutron diffractometer at the High Flux Isotope Reactor, J. Appl. Crystallogr. **44**, 655 (2011).

[13] V. Petříček, L. Palatinus, J. Plášil, and M. Dušek, JANA2020 – a new version of the crystallographic computing system JANA, Z. Kristallogr.-Cryst. Mater. **238**, 271 (2023).

[14] See Supplemental Material at http://link.aps.org/supplemental/10.1103/n3yq-b937 for details and results about magnetometry and nuclear and magnetic structure refinements.

[15] P. E. Jönsson, R. Mathieu, P. Nordblad, H. Yoshino, H. A. Katori, and A. Ito, Nonequilibrium dynamics of spin glasses: Examination of the ghost domain scenario, Phys. Rev. B **70**, 174402 (2004).

[16] P. Nordblad, Competing interaction in magnets: The root of ordered disorder or only frustration? Phys. Scr. **88**, 058301 (2013).

[17] K. Jonason and P. Nordblad, Sensitivity to temperature perturbations of the ageing states in a re-entrant ferromagnet, Eur. Phys. J. B **10**, 23 (1999).

[18] R. Mathieu, P. Jönsson, D. N. H. Nam, and P. Nordblad, Memory and superposition in a spin glass, Phys. Rev. B **63**, 092401 (2001).

[19] F. Labib, K. Nawa, Y. Nambu, H. Takakura, Y. Ikeda, K. Deguchi, M. Matsuura, A. Ishikawa, R. Kajimoto, K. Ikeuchi, *et al.*, Universal whirling magnetic orders in non-Heisenberg Tsai-type quasicrystal approximants, arXiv:2503.01517.

[20] K. K. Thilakan, F. Denoel, Y.-C. Huang, O. Fabelo, R. Mathieu, C. P. Gómez, and M. Sahlberg, Single-crystal neutron diffraction study on the $Ho_{13.6}Au_{61.1}Al_{25.3}$ quasicrystal approximant, J. Alloys Compd. **1002**, 175263 (2024).

[21] K. Nawa, M. Avdeev, A. Ishikawa, H. Takakura, C.-W. Wang, D. Okuyama, R. Murasaki, R. Tamura, and T. J. Sato, Magnetic properties of the quasicrystal approximant $Au_{65}Ga_{21}Tb_{14}$, Phys. Rev. Mater. **7**, 054412 (2023).

[22] G. H. Gebresenbut, M. S. Andersson, P. Nordblad, M. Sahlberg, and C. Pay Gómez, Tailoring magnetic behavior in the Tb-Au-Si quasicrystal approximant system, Inorg. Chem. **55**, 2001 (2016).

[23] G. M. Rotaru, B. Roessli, A. Amato, S. N. Gvasaliya, C. Mudry, S. G. Lushnikov, and T. A. Shaplygina, Spin-glass state and long-range magnetic order in $Pb(Fe_{1/2}Nb_{1/2})O_3$ seen via neutron scattering and muon spin rotation, Phys. Rev. B **79**, 184430 (2009).

[24] J. A. Paixão, M. Ramos Silva, S. A. Sørensen, B. Lebech, G. H. Lander, P. J. Brown, S. Langridge, E. Talik, and A. P. Gonçalves, Neutron-scattering study of the magnetic structure of $DyFe_4Al_8$ and $HoFe_4Al_8$, Phys. Rev. B **61**, 6176 (2000).

[25] M. Giot, A. Pautrat, G. André, D. Saurel, M. Hervieu, and J. Rodriguez-Carvajal, Magnetic states and spin-glass properties

in $Bi_{0.67}Ca_{0.33}MnO_3$: Macroscopic ac measurements and neutron scattering, Phys. Rev. B **77**, 134445 (2008).

[26] S. Mitsuda, H. Yoshizawa, T. Watanabe, S. Itoh, Y. Endoh, and I. Mirebeau, Neutron depolarization studies on reentrant spin glass AuFe alloy, J. Phys. Soc. Jpn. **60**, 1721 (1991).

[27] H. Kawamura, Chirality scenario of the spin-glass ordering, J. Phys. Soc. Jpn. **79**, 011007 (2010).

[28] S. Watanabe, Topological magnetic textures and long-range orders in terbium-based quasicrystal and approximant, Proc. Natl. Acad. Sci. USA **118**, e2112202118 (2021).

[29] T. J. Sato, A. Ishikawa, A. Sakurai, M. Hattori, M. Avdeev, and R. Tamura, Whirling spin order in the quasicrystal approximant $Au_{72}Al_{14}Tb_{14}$, Phys. Rev. B **100**, 054417 (2019).

[30] L. Balents, Spin liquids in frustrated magnets, Nature (London) **464**, 199 (2010).

[31] O. Beckman, E. Figueroa, K. Gramm, L. Lundgren, K. V. Rao, and H. S. Chen, Spin wave and scaling law analysis of amorphous $(Fe_xNi_{1-x})_{75}P_{16}B_6Al_3$ by magnetization measurements, Phys. Scr. **25**, 726 (1982).

[32] I. Mirebeau and N. Martin, Revisiting neutron studies of reentrant spin glasses: The role of small-angle scattering, J. Appl. Crystallogr. **55**, 1173 (2022).

[33] B. V. B. Sarkissian, The appearance of critical behaviour at the onset of ferromagnetism in AuFe alloys, J. Phys. F: Met. Phys. **11**, 2191 (1981).

[34] R. Padam, T. Sarkar, R. Mathieu, S. Thota, and D. Pal, Magnetic phase diagram of $Co(Cr_{1-x}Al_x)_2O_4$ ($x = 0.0$–1.0), J. Appl. Phys. **122**, 073908 (2017).

[35] D. C. Joshi, G. Gebresenbut, C. Pay Gomez, and R. Mathieu, Memory and rejuvenation in a quasicrystal, Europhys. Lett. **132**, 27002 (2020).

[36] F. Denoel, D. C. Joshi, Y.-C. Huang, G. H. Gebresenbut, C. Pay Gómez, and R. Mathieu, Magnetic frustration and glassiness in an icosahedral *i*-Tb-Cd quasicrystal, Phys. Rev. B **109**, 184425 (2024).